Received: 4 April 2023 | Revised: 16 June 2023 | Accepted: 24 June 2023

DOI: 10.1002/rra.4181

RESEARCH ARTICLE

WILEY

Terrain-derived measures for basin conservation and restoration planning

Jeremy E. Matt[1,2,3] | Kristen L. Underwood[1,3] | Rebecca M. Diehl[2,4] | K. S. Lawson[1] | Lindsay C. Worley[1,3] | Donna M. Rizzo[1,2,3]

[1]Department of Civil and Environmental Engineering, University of Vermont, Burlington, Vermont, USA

[2]Vermont Complex Systems and Data Science Center, University of Vermont, Burlington, Vermont, USA

[3]Gund Institute for Environment, University of Vermont, Burlington, Vermont, USA

[4]Department of Geography and Geosciences, University of Vermont, Burlington, Vermont, USA

Correspondence
Jeremy E. Matt, Vermont Complex Systems and Data Science Center, Innovation Hall 4th floor, 82 University Place, University of Vermont, Burlington, VT 05405, USA.
Email: jmatt@uvm.edu

Funding information
Barrett Foundation; Lake Champlain Sea Grant, University of Vermont; National Oceanic and Atmospheric Administration, Grant/Award Numbers: NA22NWS4320003, NA18OAR4170099; National Science Foundation, Grant/Award Number: EPS-1101317; Vermont Department of Environmental Conservation; University of Alabama

Abstract

Centuries of human development have altered the connectivity of rivers, adversely impacting ecosystems and the services they provide. Significant investments in natural resource projects are made annually with the goal of restoring function to degraded rivers and floodplains and protecting freshwater resources. Yet restoration projects often fall short of their objectives, in part due to the lack of systems-based strategic planning. To evaluate channel-floodplain (dis)connectivity and erosion/incision hazard at the basin scale, we calculate Specific Stream Power (SSP), an estimate of the energy of a river, using a topographically based, low-complexity hydraulic model. Other basin-wide SSP modeling approaches neglect reach-specific geometric information embedded in Digital Elevation Models. Our approach leverages this information to generate reach-specific SSP-flow curves. We extract measures from these curves that describe (dis)connected floodwater storage capacity and erosion hazard at individual design storm flood stages and demonstrate how these measures may be used to identify watershed-scale patterns in connectivity. We show proof-of-concept using 25 reaches in the Mad River watershed in central Vermont and demonstrate that the SSP results have acceptable agreement with a well-calibrated process-based model (2D Hydraulic Engineering Center's River Analysis System) across a broad range of design events. While systems-based planning of regional restoration and conservation activities has been limited, largely due to computational and human resource requirements, measures derived from low-complexity models can provide an overview of reach-scale conditions at the regional level and aid planners in identifying areas for further restoration and/or conservation assessments.

KEYWORDS
conservation, flood attenuation, flood modeling, floodplains, fluvial erosion, lateral connectivity, restoration, specific stream power

1 | INTRODUCTION

Frequent exchange of water and sediment between rivers and their floodplains supports a myriad of biogeochemical, physical, and ecological processes (Opperman et al., 2010; Tockner & Stanford, 2002; Ward, 1989; Ward & Stanford, 1995), leading to societal benefits that include sediment and nutrient storage (Noe & Hupp, 2009) and attenuation of flood waves (Akanbi et al., 1999).

However, human activities can vertically and/or laterally disconnect the channel from its floodplain, leading to adverse impacts on floodplain function and downstream water quality (Blanton & Marcus, 2009; Booth, 1990; Nilsson et al., 2005; Simon & Rinaldi, 2006). Where floodplains are disconnected or channels incised, increased stream power and excessive erosion often lead to unstable banks and high nutrient and sediment loads (Booth, 1990; Jones et al., 2000; Kline & Cahoon, 2010; Underwood et al., 2021). These effects can result in degradation of aquatic and riparian habitats via changes in water temperature, changes in water chemistry, and altered nutrient and sediment transport patterns (Holman-Dodds et al., 2003; Juan et al., 2020). Channelization and urbanization also increase the flashiness of flooding (Schoof, 1980; Shankman & Pugh, 1992) and resulting flood hazard (Kvočka et al., 2018). To counteract these effects, management planning approaches that promote 'room for the river' and the protection and restoration of floodplain connectivity are becoming increasingly popular alternatives to more traditional flood mitigation approaches, such as dams and levees (Gourevitch et al., 2020; Morris et al., 2004, 2005; Rijke et al., 2012). Unfortunately, these river and floodplain restoration efforts are often undertaken in an ad hoc manner that may limit their intended contributions (Alexander & Allan, 2007; Hermoso et al., 2012; Roni et al., 2008). Management tools that can rapidly evaluate and visualize connectivity status and channel erosion potential over a wide spatial extent provide opportunities to maximize the benefits of restoration and conservation efforts.

Assessing and understanding channel-floodplain connectivity at the basin or larger scale is a vital component of river restoration and conservation planning, regardless of the specific management goal (e.g., floodplain/river ecosystem health, control of invasive species, flood damage risk assessment, reduced sediment/nutrient transport to receiving waters). The relationship between connectivity and floodwater storage has been explored in the literature (Lane, 2017; Morris et al., 2004, 2005; Wohl, 2017), yet a method for quantifying lateral channel-floodplain connectivity at basin scales has eluded most. Flood wave attenuation is a proxy for connectivity (Acreman et al., 2003; Ahilan et al., 2018; O'Sullivan et al., 2012; Wolff & Burges, 1994), but modeling flood wave attenuation often requires process-based hydrodynamic models that are costly to develop and apply at the basin scale. Watershed sediment and nutrient budgets capture broad-scale processes, but the role of connected floodplains, relative to other processes is hard to disentangle (Gleason et al., 2007; Grauso et al., 2018; Lane et al., 2009). Wilkinson et al. (2010) provide a measure of disconnected storage capacity that may be accessed during larger design floods, but their approach relies on engineered features with known volumes. The increasing availability of high-resolution topographic datasets and low-complexity modeling approaches (Ahmad, 2018; Danielson, 2013; Diehl et al., 2021; Jain et al., 2006; Nobre et al., 2011; Reinfelds et al., 2004; Wechsler, 2007; Zheng et al., 2018) offer the potential to examine channel-floodplain connectivity at the basin scale in a more direct, and relatively rapid manner.

Specific stream power (SSP) has been successfully estimated at scale to approximate sediment transport characteristics and assess erosion potential and channel stability (Bagnold, 1966; Beck et al., 2019; Bizzi & Lerner, 2015; Booth, 1990; Knighton, 1999; Magilligan, 1992; Nanson & Croke, 1992; Wilson et al., 2007). Watershed-scale models that use SSP to evaluate areas of erosion hazard often use digital elevation models (DEMs) in conjunction with basin regression equations for streamflow (Ahmad, 2018; Danielson, 2013; Jain et al., 2006; Reinfelds et al., 2004). These DEM-based models typically use slope and flow accumulation area to provide valuable information on the distribution of floodwater energy within a watershed but neglect reach-specific geometric information. Zheng et al. (2018) describe methods for approximating reach geometry from the height above nearest drainage (HAND) maps of Nobre et al. (2011) to estimate discharge. Diehl et al. (2021) use a similar method as the basis for their low-complexity probabilistic inundation model (probHAND).

In this manuscript, we leverage the information encoded in DEMs and relative elevation products to estimate reach-specific SSP patterns and associated measures that can be calculated rapidly across basin scales. We present a method of estimating SSP using a low-complexity hydraulic model and compare SSP estimates to those of a calibrated 2D hydrodynamic model. Plots of variation in SSP with increasing flow rate at the reach scale were used to extract process-form measures of floodplain connectivity and functioning, including water storage and fluvial erosion hazard. We hypothesize that such process-form measures may be used as a reasonable alternative to labor-intensive manual geomorphic assessment. Since our measures may be rapidly generated over large spatial areas, they can serve as a management tool to optimize efforts to enhance lateral connectivity, attenuate floodwaters, and reduce fluvial erosion.

2 | METHODS

The following sections introduce the study area and describe methods for (i) producing curves that describe changes in stream reach SSP with increasing discharge using a low-complexity hydraulic model; (ii) verifying low-complexity SSP values using a calibrated, process-based model (i.e., 2D HEC-RAS); and (iii) extracting process-form measures at the reach scale.

2.1 | Study area

To illustrate our framework, we chose the Mad River watershed located in central Vermont (Figure 1), due to the abundance of prior work related to stream geomorphic conditions and processes (Ross et al., 2019; Worley et al., 2023) and the availability of a well-calibrated 2D HEC-RAS model for assessing our low-complexity model results (Seigel, 2021; Worley et al., 2022). Elevations in the Mad River watershed range from 132 to 1245 m above sea level. Land use is primarily forested, with agriculture and village centers concentrated along the valley bottom lands. Our study focused on

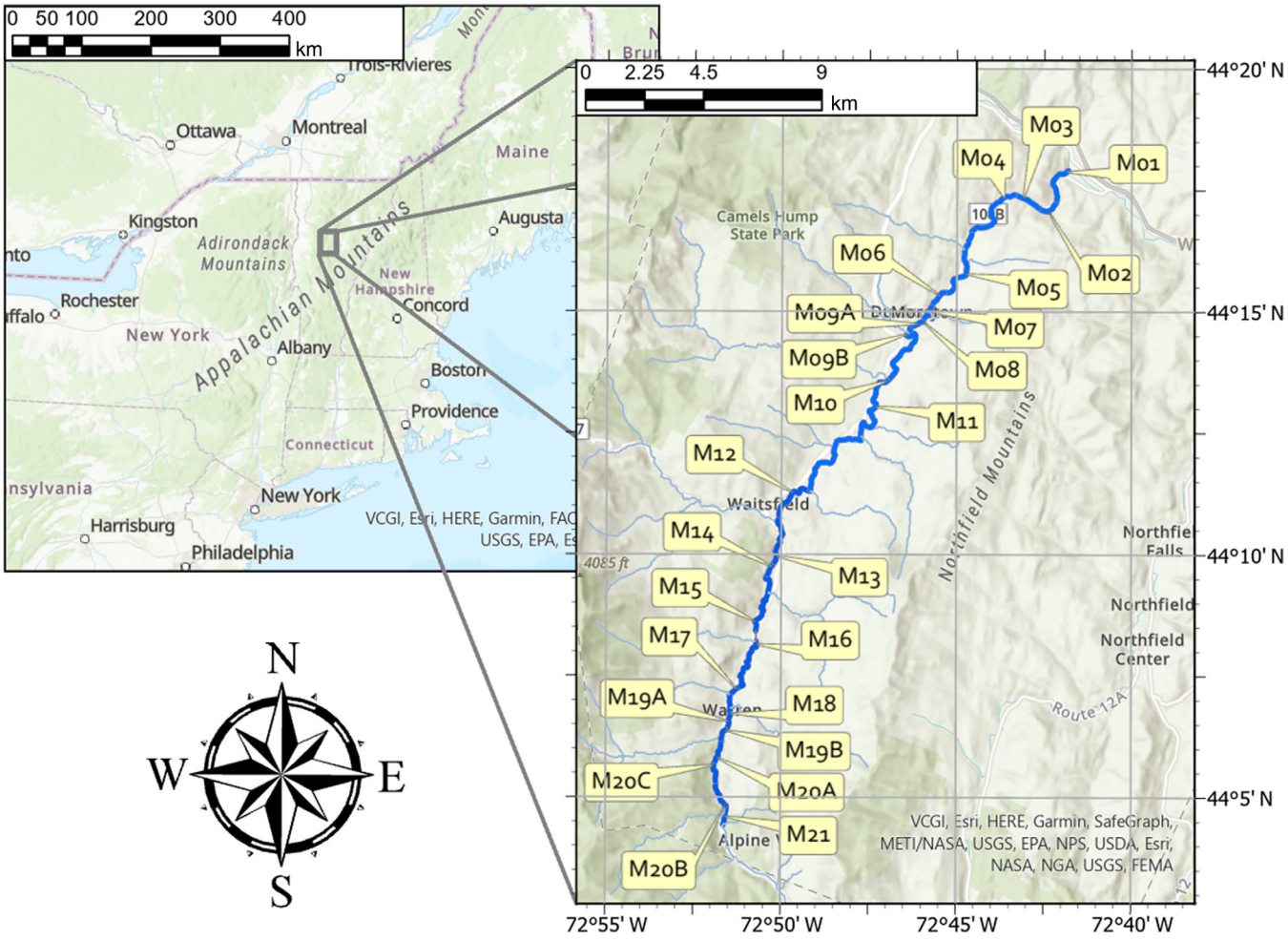

FIGURE 1 The study area comprises 25 reaches along the main stem of the Mad River in central Vermont (dark blue). The remainder of the river network not included in this study is shown as thin, lighter blue lines. Reach labels (M01 through M21) indicate reach positions in the study area. [Color figure can be viewed at wileyonlinelibrary.com]

25 main stem reaches defined by the Vermont Stream Geomorphic Assessment (SGA; see Supplemental S.1a) along a 38-km stretch of the Mad River. Reach drainage areas range from 31.9 to 373 km^2. The SGA reach breaks are selected to separate lengths of channel that are geomorphically consistent, meaning they display internally consistent valley confinement, slope, sinuosity, and vertical/lateral connectivity status (Kline et al., 2009; Underwood et al., 2021). Reach slopes range from 1.97% in the steeper, confined bedrock-controlled gorges to 0.15% in shallower-gradient, unconfined, alluvial settings; reach lengths vary from 0.2 to 7.1 km. Of the 25 reaches in the study area, one is impounded and was, therefore, excluded from further analysis. Six (24%) are bedrock-controlled, and the remaining 18 (72%) are alluvial channels. Reaches vary in their degree of valley confinement from 1.3 to 16 times the channel width. Entrenchment ratios varied from 1.13 to 12. Channel management activities (dredging, straightening, damming, road/berm construction, and armoring) that occurred as recently as the mid-20th century have reduced access to floodplains in some reaches via encroachment and channel incision (Fitzgerald & Godfrey, 2008).

2.2 | Development of SSP-flow curves

2.2.1 | Reach-averaged SSP using a low-complexity hydraulic model

We calculated SSP using the probHAND model, a low-complexity DEM-based model that extends the HAND model (Nobre et al., 2011). The probHAND model includes a Monte Carlo simulation that accounts for measurement uncertainty and errors associated with simplifying assumptions (Diehl et al., 2021). Inputs to the probHAND model included: LiDAR-derived DEM rasters (1 m resolution), a land-use land-cover (LULC) raster layer (1 m resolution), stream reach polylines, channel bed grainsize distributions, and design flood flow rate data for each stream reach. Data sources and acquisition dates are provided in Supplemental S.2.

We calculated SSP (watts/m^2) as the product of the reach-averaged flow rate (Q [m^3/s]), reach slope (s [m/m]), and specific weight of water ($\gamma = 9810$ kg/m^{2}s^2), all divided by the average channel width (W [m]) of each stream reach:

$$SSP = \frac{\gamma Qs}{W}. \quad (1)$$

Discharge was calculated using reach-averaged parameters for the Manning equation after Diehl et al. (2021). For a given stage (Figure S.1; see Supplemental S.3), reach-averaged discharge was calculated as:

$$Q = \frac{AR^{2/3}\sqrt{s}}{n_w}, \quad (2)$$

where A (m^2) is the reach-averaged cross-sectional area of flow, R (m) is the hydraulic radius, s (m/m) is the slope calculated from reach length and minimum and maximum DEM elevations, and n_w ($s/m^{1/3}$) is the weighted Manning roughness coefficient. The method of determining A, R, s, and n_w is described in Supplemental S.3. An evaluation of the relationship between SSP, Q, and channel geometry is provided in Supplemental S.3a.

To evaluate whether the assumption of normal depth flow conditions affects SSP estimation, we benchmarked the SSP calculated from probHAND using a calibrated two-dimensional Hydraulic Engineering Center's River Analysis System (HEC-RAS) unsteady model of the study area (Seigel, 2021; Worley et al., 2022). We ran the HEC-RAS model for 2-, 25-, 50-, 100-, and 500-year design events (Q2, Q25, Q50, Q100, and Q500) and exported rasters of SSP for each event. Average SSP was calculated for each reach by averaging the SSP raster within the probHAND Thiessen polygon corresponding to that reach (Figure S.2; see Supplemental S.4). We also calculated reach-averaged channel- and overbank-specific SSP values using top-of-bank lines present in the HEC-RAS model to separate channel and overbank areas (Figure S.2; see Supplemental S.4). We compared the channel, overbank, and total reach probHAND SSP values to the corresponding HEC-RAS SSP values on a reach basis, using root-mean-square error (RMSE) and relative percent difference (RPD).

2.2.2 | Development of SSP-flow curves

To visualize how SSP varies with flow of different magnitudes, we plotted probHAND SSP versus Q for 100 stage heights between 0 and 10 m above the channel. We normalized Q by the Q2 flow rates derived from regional flood frequency regressions (Olson, 2014) to compare SSP versus Q patterns between reaches. We display normalized Q values between zero and six times the Q2 flow rate to highlight flood sizes most important in design practice (in this work: Q2, Q25, Q50, Q100, and Q500). We refer to these as 'SSP-flow curves' throughout the remainder of the paper (Supplemental S.5). We separated the SSP-flow curves into channel and overbank areas using the LULC layer (Supplemental S.3).

2.3 | Development and evaluation of form-process measures

We relied upon SSP-flow curves to develop three form-process measures that: (i) reveal patterns of energy dissipation as flood stage is incrementally increased for each channel/floodplain geometry, (ii) estimate connected and disconnected flood water storage capacities and (iii) characterize fluvial erosion hazard relative to a critical SSP threshold. Next, we compared these form-process measures with available reach geomorphic information (e.g., categories of valley confinement, incision, and entrenchment and degree of built infrastructure encroaching within the floodplain) to correlate patterns with channel-floodplain geometry.

2.3.1 | Characterizing spillover patterns and the design flood at which spillover occurs

The first measure uses the shape and slope of the SSP-flow curves to characterize three types of spillover patterns indicative of the degree and nature of floodplain access and associated energy dissipation. The first spillover pattern is characterized by a 'Gradual' flattening or modest drop in SSP with increasing stage/discharge. The second pattern, referred to as 'Abrupt' spillover, is characterized by a relatively large change in the slope of the SSP-flow curve, indicative of a large decrease in SSP associated with either a reduction in Q or discharge that remains nearly constant. The third pattern is characterized by a lack of spillover and monotonically increasing SSP (e.g., reach M01 in Supplemental S.5). We automated the categorization of the spillover type based on the slope of the SSP-flow curves (Supplemental S.6). An abrupt spillover was characterized by a very-large-magnitude slope value. A gradual spillover was characterized by a slope value slightly above or below zero. To characterize the frequency of spillover in each reach, we linked each spillover event to a flood stage at which spillover first occurs and called that the 'First Spillover Design Flood'.

2.3.2 | Classifying floodplain storage capacity

We calculated floodplain storage capacity of each reach as a specific volume capacity (m^3/m)—defined as the total volume in a reach divided by reach length (Castellarin et al., 2011); normalizing by reach length allowed for comparison between reaches of different lengths. We then classified two forms of floodplain storage capacity based on the SSP-flow spillover patterns. Connected Specific Volume Capacity (CSVC) is associated with gradual spillover patterns and suggests natural channel-floodplain connectivity. Whenever gradual spillover was identified in a given reach, we calculated the floodwater volume of each spillover event and associated these volumes with design floods (see Supplemental S.6a).

Disconnected Specific Volume Capacity (DSVC) is the volume of all 'closed topographic depressions' (Lindsay, 2016) below a given flood stage normalized by the reach length. It suggests either natural topographic depressions on the landscape (e.g., wetlands) or areas disconnected from the river by unnatural features (e.g., road berms). We refer to closed topographic depressions (i.e., low-lying areas below the surrounding topography) as 'pits' for the remainder of this paper. DEM pit-filling is commonly performed in low-complexity hydraulic modeling and hydrologic analyses to ensure that stream network

elevations do not increase from upstream to downstream (Zheng et al., 2018). To satisfy this constraint, DEM pits must be 'filled' to the pour point, which is the lowest point on the terrain boundary draining into the pit (Lindsay, 2016; Nobre et al., 2011). As a result, pits are replaced with a flat surface equal in elevation to the pour point. This surface is subsequently transferred to the HAND elevation raster.

To estimate the DSVC of each reach, we extracted the DEM pit topography, restored that pit-filled floodplain topography to the HAND elevation raster, and finally compared this restored topography to flood stages (as done in Section 2.2.1 when estimating Q). This process is shown in Figure 2. We first identified floodplain locations in the DEM that were 'pit filled' (Figure 2, hatched area in panel a) and compared these with the original DEMs. The difference in elevation between the original DEM (panel b) and the pit-filled DEM (panel a) for each cell in the landscape represents the 'depth' of pit filling: any cells with a value greater than 0 (gray shaded plan view areas in panel c) were pit filled. Pit-filled 'depths' were extracted (Figure 2, panel e) from the HAND elevation raster (panel d) to approximate a HAND elevation raster for the pit-filled areas. As with the original HAND raster, any pit topography cells in the HAND raster with an elevation less than the inundation stage were considered inundated. Thus, any pit topography cells inundated in the updated HAND raster, but not in the original HAND raster, were defined as disconnected. The disconnected volume for a given stage (Figure S.3; see Supplemental S.7) is the sum of all disconnected volume(s) below the flood stage.

2.3.3 | Critical SSP threshold exceedance measure

Critical SSP threshold values describe energy levels that are related to the potential of significant channel bed erosion for alluvial reaches. To assess the erosion hazard for a given reach, we compared the in-channel SSP-flow curve to a critical SSP threshold value defined in Equation (3). Using pebble count data available from SGA assessments (VTANR, 2022), we estimated the critical SSP threshold (SSP_{crit}) for the 84th percentile of the bed grain size distribution (D_{84}) after Ferguson (2005):

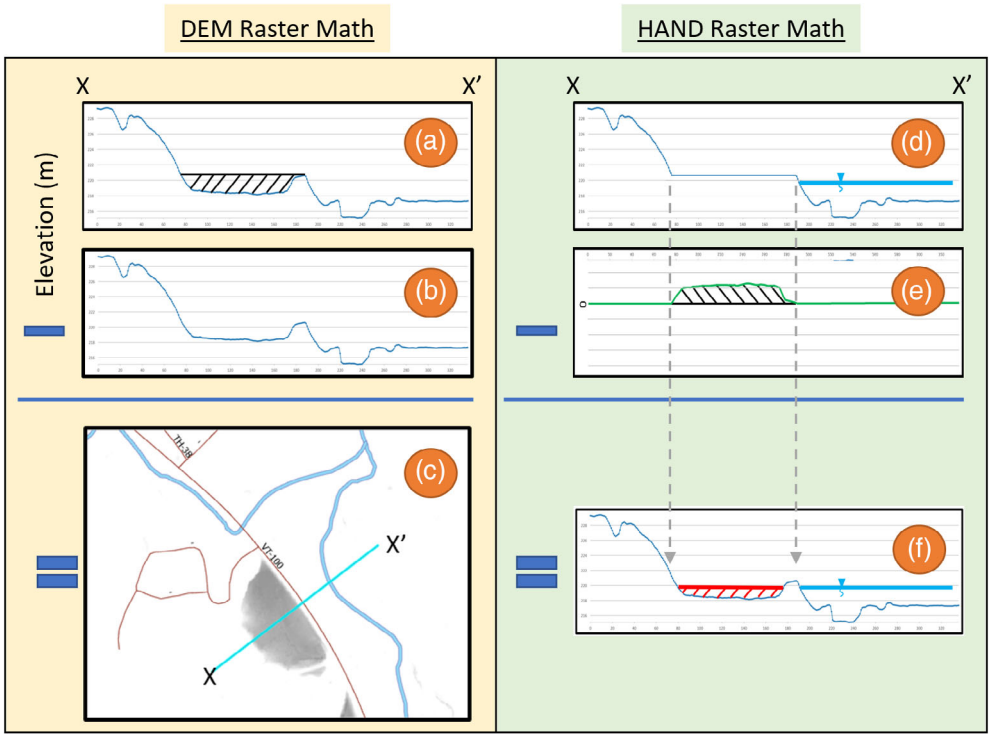

FIGURE 2 Schematic showing the raster math operations used to calculate the volume of closed topographic depressions (pits) and restore them to the HAND raster layer. The X–X′ transect referred to is identified in (c). The pit-filled digital elevation model (DEM) elevations along the X–X′ transect are shown in (a); the hatched area represents the pit-filled depths along the transect. The original DEM elevations along the X–X′ transect are shown in (b). The sample area shown in (c) includes a floodplain area (shaded in gray) that is disconnected from the river by a road embankment. The elevations of the HAND raster (generated from the pit-filled DEM) along X–X′ are shown in panel d. Using a DEM raster math operation, from (a), we subtract the original DEM (b) to generate a raster of pit-filled 'depths' (panel c in plan view; panel e in transect view). From the HAND raster (d), we then subtract the pit-filled 'depths' along the X–X′ transect (e) to obtain an updated HAND raster with pits restored (f). The red line in panel f represents the elevation of the example water surface (represented by the thick blue line in d and f) in the pit-filled area if the road embankment was not present. The disconnected volume of this feature for the stage shown in (f) is the volume between the water surface elevation (red line) and the estimated HAND topography in the pit-filled area. [Color figure can be viewed at wileyonlinelibrary.com]

$$SSP_{crit} = 0.113 * D_{50}^{1.5} * \log\left[\left(\frac{0.73}{s}\right) * \left(\frac{D_{84}}{D_{50}}\right)^{0.4}\right]\left(\frac{D_{84}}{D_{50}}\right)^{0.4}, \quad (3)$$

where s is the channel slope, and D_{50} is the 50th percentile particle diameter in mm (Andrews, 1983). The 95% confidence intervals for the D_{50} and D_{84} diameters were generated from the cumulative grain-size distribution (the horizontal red and yellow arrows, Figure S.4; see Supplemental S.8). The SE around the percentile (p = 50th or 84th) was calculated after Eaton et al. (2019) from field survey data as:

$$\sigma_p = \sqrt{\left(\frac{p}{100}\right) * \left(1 - \frac{p}{100}\right) * \frac{1}{N}}, \quad (4)$$

where N is the number of grains counted during the grainsize survey.

The upper and lower 95% confidence intervals on the target particle diameter were calculated as:

$$UCL = p + 1.96 * \sigma_p, \quad (5)$$

$$LCL = p - 1.96 * \sigma_p. \quad (6)$$

Linear interpolation of the cumulative grainsize distribution curve, plotted as percentile versus $\log_2(D)$, provided nominal diameters for the D_{50} and D_{84} as well as upper and lower 95% confidence intervals (UCL and LCL, respectively) for the D_{50} and D_{84}. See vertical $LOG_2(p_{84,ucl})$, $LOG_2(p_{84})$, and $LOG_2(p_{84,lcl})$ arrows in Figure S.4. We used the nominal values for D_{50} and D_{84} and their respective UCL and LCL to calculate SSP_{crit} and the approximate upper and lower 95% confidence intervals (UCL and LCL, respectively). To assess the hazard of channel bed erosion, we compared the channel SSP at each design flood to the critical SSP threshold and its UCL and LCL.

2.3.4 | Statistical analysis and qualitative comparisons

We performed a non-parametric Kruskal-Wallis test (SciPy, 2019) to explore the relationship of SGA parameters (i.e., Entrenchment and Incision Ratios) with our three measures (i.e., SSP Threshold Exceedance, presence/absence of CSVC values >0, and DSVC values >1.0; Table S.1) at flows below the Q50. We used a threshold of 1.0 for DSVC because small values appeared to be associated with micro-topography and/or noise in the DEMs rather than disconnected energy dissipation areas. We disregarded the presence of CVSC, DSVC, and Critical SSP threshold exceedances above the Q50 because designing for such low-frequency, high-intensity storms is typically outside the scope of restoration and conservation projects that these tools are intended to support. We evaluated the importance of the presence of bedrock controls, valley confinement ratio (VC; valley width divided by bankfull channel width), entrenchment ratio (ER; flood-prone width divided by bankfull width), incision ratio (IR; low bank height divided by bankfull height), and road encroachment (Supplemental S.1b).

2.4 | Computation

All analyses were performed on a Dell XPS9700 laptop with 64GB of RAM using Python 3 and TauDEM 5.3.7 (Tarboton, 2016). The Python code used in this work is available at https://github.com/jeremymatt/terrain_derived_connectivity_measures.

3 | RESULTS

3.1 | Verification of probHAND SSP estimates

We observed that the probHAND model systematically overestimated SSP for the channel (22.6% RPD on average; Figure 3, panel a) and underestimated overbank SSP (44.2% RPD on average; Figure 3, panel c). When considering the combined channel and overbank estimates, these effects offset each other, and SSP values were similar to the HEC-RAS SSP values on average, differing by only 8% RPD (Figure 3, panel c). Underestimation of probHAND SSP was especially apparent for one reach, M03 (the outlier in panels a, b, and c). However, this reach is impounded by a run-of-river hydroelectric dam and was therefore excluded from the RMSE and RPD calculations summarized in Figure 3, panel d.

3.2 | Relationship of process-form measures to channel-floodplain geometry and SGA parameters

3.2.1 | Spillover patterns and the design event at which spillover occurs

The frequency and type of spillover shown in the SSP-flow curve reflect presence, scale, and (dis)connectivity of floodplain features across the range of study reaches. Of the 18 alluvial reaches, 8 (44%) first experience spillover (Gradual and/or Abrupt) at or below the Q50 (Table S.1) in a portion of the flow regime characterized by lower magnitude, higher frequency floods and VCs greater than 5. We use the Q50 as a breakpoint between smaller events that are easier to design for, and infrequent events that are likely to cause substantial damage regardless of restoration/conservation efforts. Two of these 8 reaches exhibit both Gradual (Figure 4) and Abrupt (Figure 5) Spillover. The occurrence of spillover at flow rates below the Q50 was positively associated with ER at the 95% confidence level (Kruskal–Wallis p = 0.020). The remaining 10 alluvial reaches (56%) did not experience spillover until flows were above the Q100 or Q500 flowrates or showed no spillover for the flows tested. This finding suggests a degree of floodplain disconnection or limited floodplain presence, given that a much larger event (of lower expected frequency) is

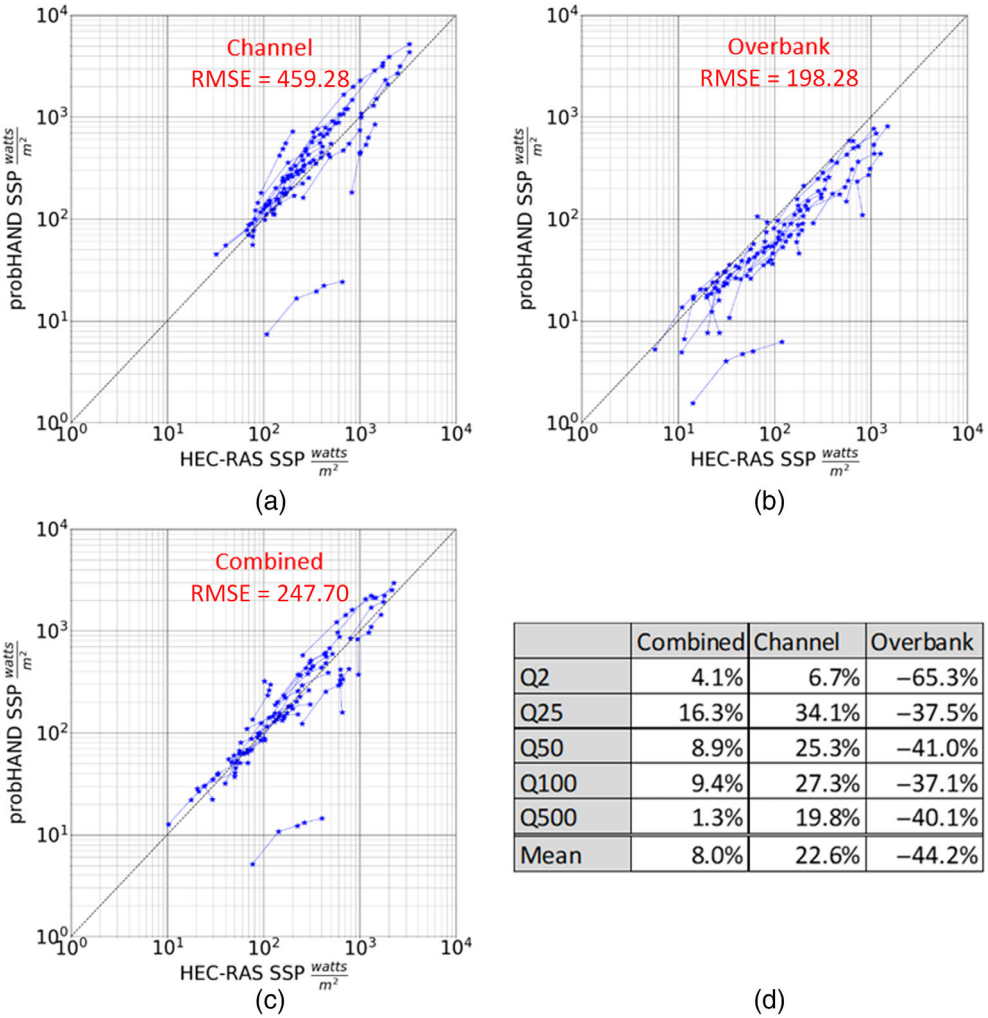

	Combined	Channel	Overbank
Q2	4.1%	6.7%	−65.3%
Q25	16.3%	34.1%	−37.5%
Q50	8.9%	25.3%	−41.0%
Q100	9.4%	27.3%	−37.1%
Q500	1.3%	19.8%	−40.1%
Mean	8.0%	22.6%	−44.2%

FIGURE 3 Log–log plots of probHAND specific stream power (SSP) versus 2D Hydraulic Engineering Center's River Analysis System (HEC-RAS) SSP and a table of mean relative percent difference values. Individual panels compare SSP for (a) the channel only, (b) the overbank only, and (c) the combined channel and overbank. Channel flow is calculated as $Q_{ch} = Q_{total} - Q_{OB}$. Each of the blue lines connects estimates for the Q2, Q25, Q50, Q100, and Q500 design storms in a single reach. The root mean square error (RMSE) values (in red at the top of each plot) and the mean relative percent differences presented in (d) exclude results for reach M03 (the outlier reach that falls well below the 1:1 line in all three plots), which is impounded and controlled by a run-of-river dam. [Color figure can be viewed at wileyonlinelibrary.com]

required to generate spillover. Reaches with No Spillover at any stage were closely confined by valley walls and had negligible floodplain extent. With one exception, these reaches had VCs less than five. They were also typically located closer to the headwaters or classified as transport-dominated reaches with bedrock channel boundaries (spillover was not observed in any of the bedrock-controlled reaches).

3.2.2 | Floodplain storage capacities

As expected, floodplain storage capacities were related to confinement status and presence/absence of spillover patterns. The CSVC values for our study area range between 0 and 200 m^3/m and between 0 and 31 m^3/m for DSVC. These measures appear to be correlated with the longitudinal position in the watershed (Figure 6). First, the six upstream reaches lack either CVSC or DVSC (defined as less than 1 m^3/m) at the Q50 or smaller and are more likely to exceed critical SSP thresholds at smaller, more frequent design storms. Conversely, 9 of the 12 most downstream alluvial reaches have more than 8 m^3/m DSVC or CSVC at these flows. These reaches also tend to be less likely to exceed critical SSP thresholds at smaller design storms. We found ER to be positively associated with the presence of both CSVC ($p = 0.049$) and DSVC ($p = 0.026$) at or below the Q50 (see Figure 7). Incision ratio was not correlated with either DSVC or CSVC ($p > 0.268$; Figure 7).

3.2.3 | Critical SSP threshold exceedance

For the alluvial study reaches, the highest in-channel SSP values occurred in the headwaters (Figures 6 and 8). Six of the seven confined alluvial reaches with greater than average slopes (0.010–0.018 m/m) had higher SSP values than the unconfined reaches with shallower slopes. While critical SSP estimated on a reach-by-reach basis varied widely, it generally decreased from upstream to downstream (Figure 8 and Supplemental S.9). The headwater reaches (M17–M21) experienced the greatest magnitude of threshold exceedances (including UCL exceedances), followed by the most downstream reaches (M01–M10) which included exceedances of the critical SSP values but not UCL exceedances. The mid-watershed reaches (M11–M16) exhibited the least erosion hazard with no exceedances of the LCL at or below the Q50. Downstream of two bedrock

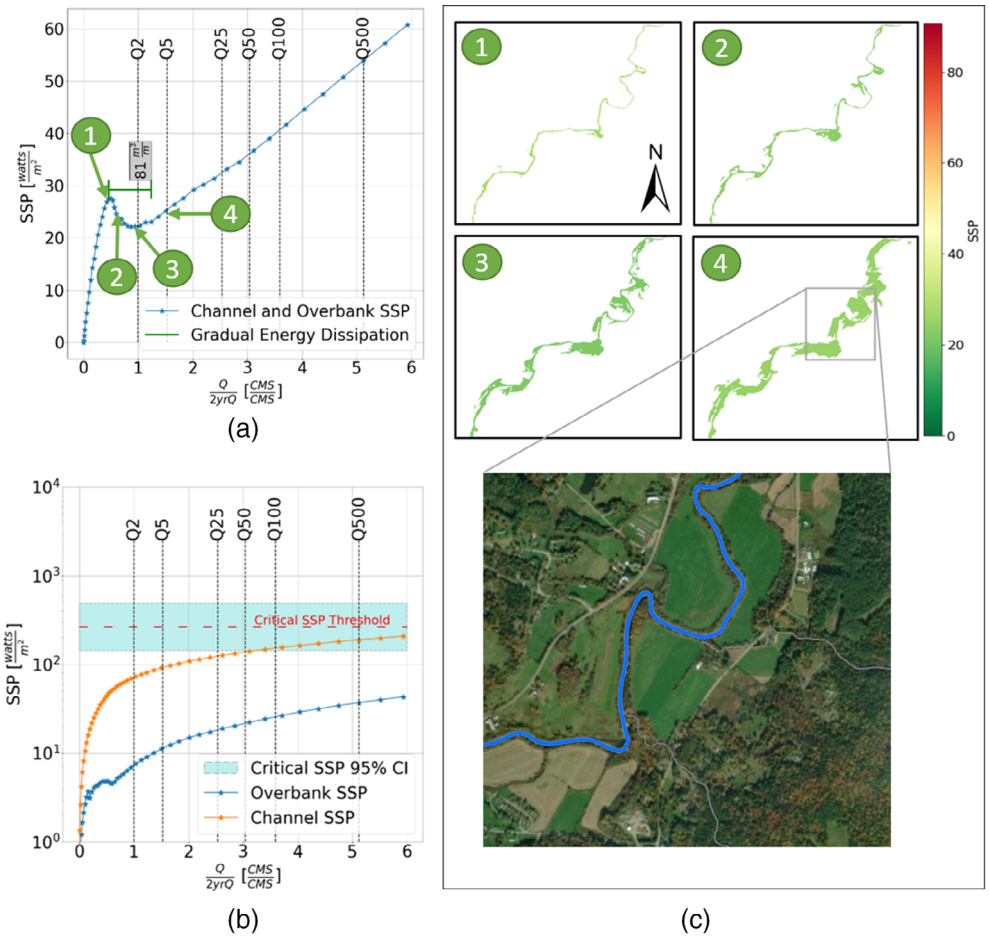

FIGURE 4 A reach exhibiting a pattern associated with gradual energy dissipation (each node of the curve represents specific stream power [SSP] and normalized discharge [Q] associated with a unique inundation stage, that monotonically increases by an increment of 0.1 m). The SSP-flow curve for the entire reach (a) and a green bracket outlining automated delineation of a gradual energy dissipation event following the method described in Section 2.3.1 with associated connected specific volume capacity of 81 m^3/m. Overbank and channel SSP-flow curves are shown in (b), along with reach-specific critical SSP thresholds. The red dashed line in (b) marks the critical SSP threshold estimated for the D_{84}. The teal band represents the approximate 95% confidence limit of the Critical SSP Threshold estimate. The channel SSP-flow curve is compared to these thresholds and to design flood flow rates to estimate erosion risk. Panel c consists of four plan-view inundation plots (corresponding to the four points marked on the curve in panel a) and an orthophoto of a representative portion of the reach. The dark blue line in the orthophoto in (c) represents the river channel. CI, confidence interval. [Color figure can be viewed at wileyonlinelibrary.com]

reaches (M17 and M18), the slopes of the alluvial reaches flatten substantially (slopes < 0.005) leading to reduced channel SSP values (Figure 8). Certain reaches (i.e., M06, M12, M14, M15, and M16) have more well-graded bed compositions (see grainsize distributions in Supplemental S.7), which result in wider ranges between the LCL and UCL and more uncertainty regarding the actual Critical SSP value (Figure 8). The wider LCL/UCL ranges were often associated with inputs from major tributaries and proximity to bedrock-controlled reaches.

SSP LCL Threshold exceedances that occur prior to the Q50 design flood tend to be associated with a lack of storage volume capacity. Of the 18 alluvial reaches, 10 exceed the LCL prior to the Q50; 6 of these 10 reaches (60%) lack connected storage capacity (CSVC/DSVC < 1 m^3/m) at these flow rates. Of the other eight alluvial reaches that do not exceed the LCL prior to the Q50, only two reaches (25%) have storage capacities of less than 9 m^3/m. While not statistically significant, visual inspection of the table in Supplemental S.9 also suggests a relationship between SSP Threshold exceedance and Entrenchment Ratio. Of the 12 entrenched reaches (ER < 3), 8 exceed the LCL prior to the Q50, while only one of 6 non-entrenched reaches (ER > 3) exceeds a critical SSP Threshold prior to the Q50. We also found no significant correlation between IR and Threshold Exceedances ($p = 0.268$; Figure 7).

4 | DISCUSSION

In this study, we mined information encoded in DEMs to extract process-form measures of floodplain connectivity and functioning, including both DSVC and CSVC, and measures of fluvial erosion hazard that may be calculated rapidly across large scales (e.g., watersheds, states, and regions). These measures help to

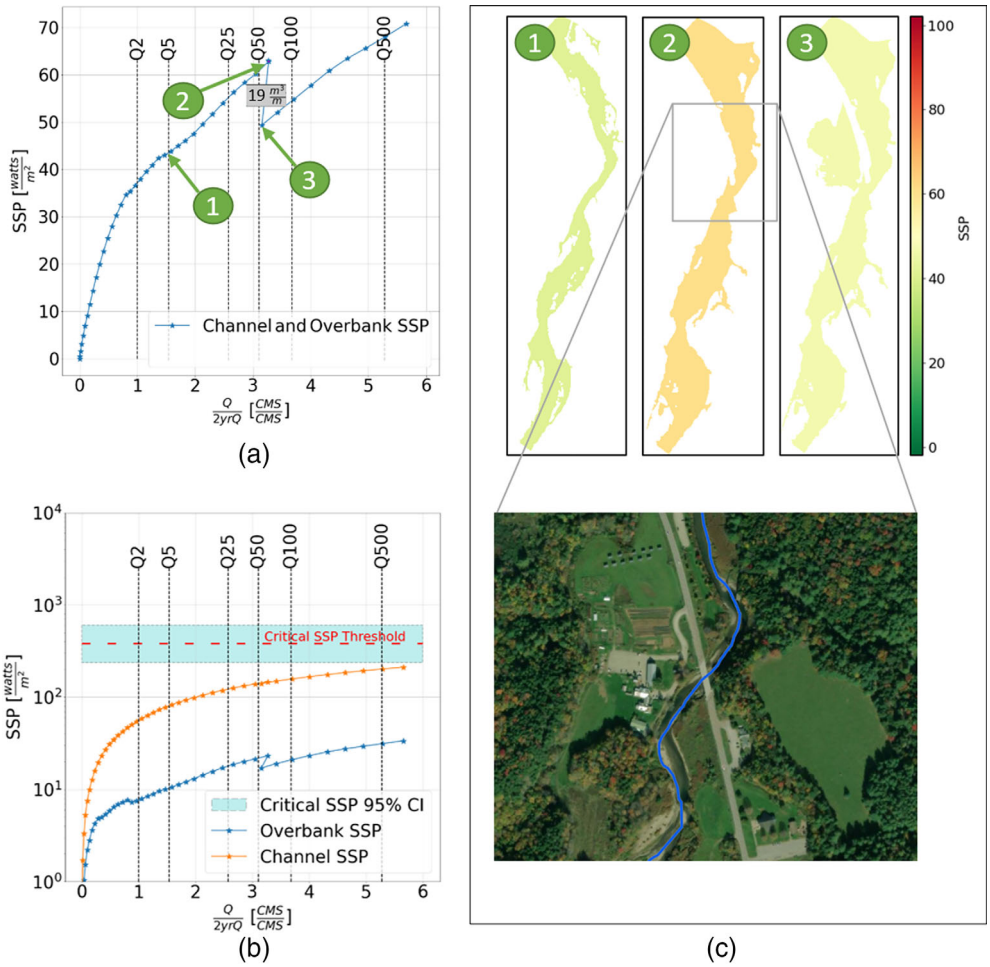

FIGURE 5 An example of typical abrupt spillover. The specific stream power (SSP)-flow curve for the entire reach is shown in (a). In (b), SSP has been divided into channel and overbank curves; the red dashed line marks the critical SSP threshold estimated for the D_{84}. The teal band represents the approximate 95% confidence limit of the Critical SSP Threshold estimate. The channel SSP-flow curve is compared to these thresholds and to design flood flow rates to estimate erosion risk. Panel c consists of three plan-view inundation plots (corresponding to the three points marked on the curve in panel a) and an orthophoto of a representative portion of the reach. The dark blue line in the orthophoto in (c) represents the river channel. Between point 2 and point 3 in (a), the pit formed by the Route 100 embankment is overtopped, allowing the river to access the formerly disconnected floodplain (C3). This pit dominates the DSVC of 19 m^3/m shown in (a). This energy dissipation results in a decrease in SSP. CI, confidence interval. [Color figure can be viewed at wileyonlinelibrary.com]

identify and rank the potential of improved function of stream reaches for conservation and restoration planning and represent a novel use of a new generation of low-hydraulic-complexity topographic-based tools (Diehl et al., 2021; Zheng et al., 2018). Increasing availability of high-resolution geospatial datasets has supported the development and implementation of these tools at broad scales, notably HAND-based approaches for flood mapping and flood hazard assessment (Diehl et al., 2021; Gourevitch et al., 2020, 2022). We demonstrate the extended applicability of HAND-based approaches, which may be broadly adopted to inform river condition and function.

Reach-averaged SSP values obtained from probHAND show similar trends to those obtained from a calibrated 2D HEC-RAS model, and differences between the two methods are likely to not alter the interpretation as applied to broad-scale planning applications (Figure 3, panel d). The approach was developed to be applied over broad scales, such as the Vermont portion of the Lake Champlain drainage basin (~4600 square miles or ~7400 sq km) for purposes of reach prioritization and watershed planning. Constructing, calibrating, and running 2D HEC-RAS or similar process-based models for these areas is highly resource intensive and would likely require years, considering the work necessary to parameterize, calibrate, and verify the several models required to cover the same expanse of study area. We found that the low-complexity probHAND results tend to be conservative, overestimating channel erosion hazard (Supplemental S.9), a preferred bias for broad-scale screening tools. Other metrics, including connected and disconnected volume, are based on flood stage (Figure 2 and Supplemental S.3a), and therefore not sensitive to differences in SSP. Once potential restoration or conservation projects are identified using our broad-scale screening approach, a given project would proceed through more rigorous engineering design that would include process-based hydraulic modeling to verify SSP and

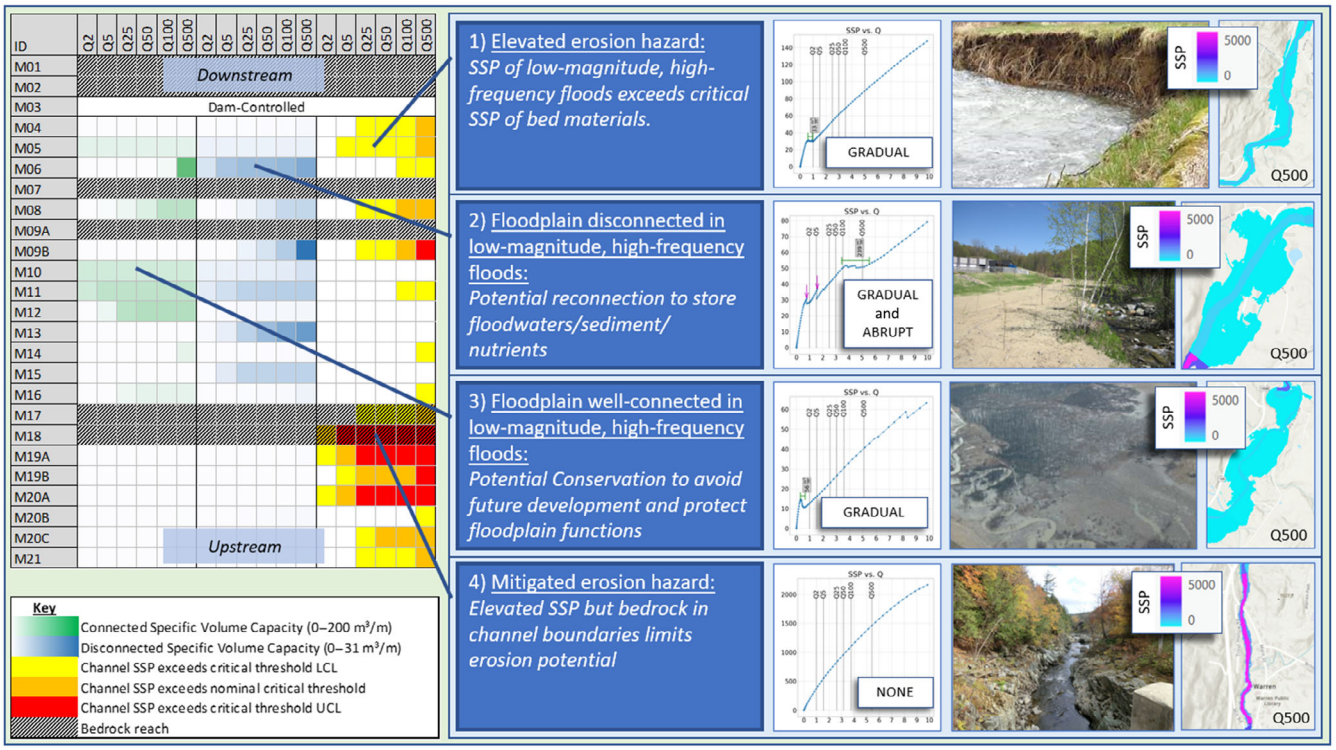

FIGURE 6 Framework illustrating the utility of process-form measures to inform river management. For each reach (i.e., row in the table to the left), the green and blue gradients in left and middle columns of the table reflect the relative connected and disconnected specific volume capacities (CSVC and DSVC), respectively. The yellow, orange, and red cells in the right column indicate exceedances of the lower confidence limit (LCL), nominal critical specific stream power (SSP) threshold, and upper confidence limit (UCL), respectively. Table S.1 provides specific values. Four example reaches are highlighted to demonstrate how information in the table may be used to identify appropriate interventions. For each example, the SSP-flow curve (with labels indicating the type of energy dissipation present) and map of probHAND inundation associated with the 500-year flood are provided for context. The above photographs were chosen to best illustrate the restoration or conservation concepts and do not necessarily reflect the actual study reach. [Color figure can be viewed at wileyonlinelibrary.com]

connectivity trends under various restoration or conservation scenarios.

Our SSP-flow curves were inspired by Magilligan (1992), who charted shear stress across a range of normalized design floods and related these curves to geomorphic setting of reaches in southwestern Wisconsin. We have extended this work to develop a method capable of generating reach-specific SSP-flow curves across broad scales for use in prioritizing reaches for potential restoration or conservation projects. We improve upon other broad-scale SSP assessments (Bizzi & Lerner, 2015; Gartner et al., 2015; Marcinkowski et al., 2022) by linking measured channel-floodplain geometry to emergent patterns in the SSP-flow curves. Other methods neglect this information resulting from interactions between flood stage and channel/floodplain geometry (Ahmad, 2018; Danielson, 2013; Jain et al., 2006; Reinfelds et al., 2004).

4.1 | Novel use of low-complexity hydraulic models can inform river condition and function

Comparing critical SSP thresholds calculated from channel bed grain-size distributions to SSP values associated with design floods provides reach-specific estimates of the frequency of channel-altering flows. In addition, the degree of erosion associated with a particular event will depend on how long the channel SSPs are elevated above critical thresholds (Lisenby et al., 2018; Magilligan et al., 2015). We conjecture that the SSP-flow curves may be used to convert hydrographs into reach- and event-specific SSP profiles and that the area between the SSP profiles and alluvial erosion threshold(s) may provide valuable estimate(s) of the erosion hazard posed by a particular flood profile.

Channel-floodplain reach configurations and the presence and influence of built infrastructure on floodplain conveyance and function may be broadly inferred based on the SSP-flow curve patterns (Figures 4 and 5, Supplemental S.5). Gradual Spillover patterns were associated with unconfined settings and wide floodplains that were relatively unobstructed by roads, berms, or other infilling development (Figure 4c). This unobstructed flow of water onto floodplains was characterized by a gradual dissipation of stream energy as the stage increased (Figure 4c). Abrupt Spillover patterns (Figure 5c) also occurred in unconfined settings with wide floodplain. However, this pattern was associated with substantial lateral/vertical disconnection between channel and floodplain, as signified by ER <3. Floodplains that experience gradual spillover at smaller First Spillover Design Floods have a more frequent exchange of water and sediment

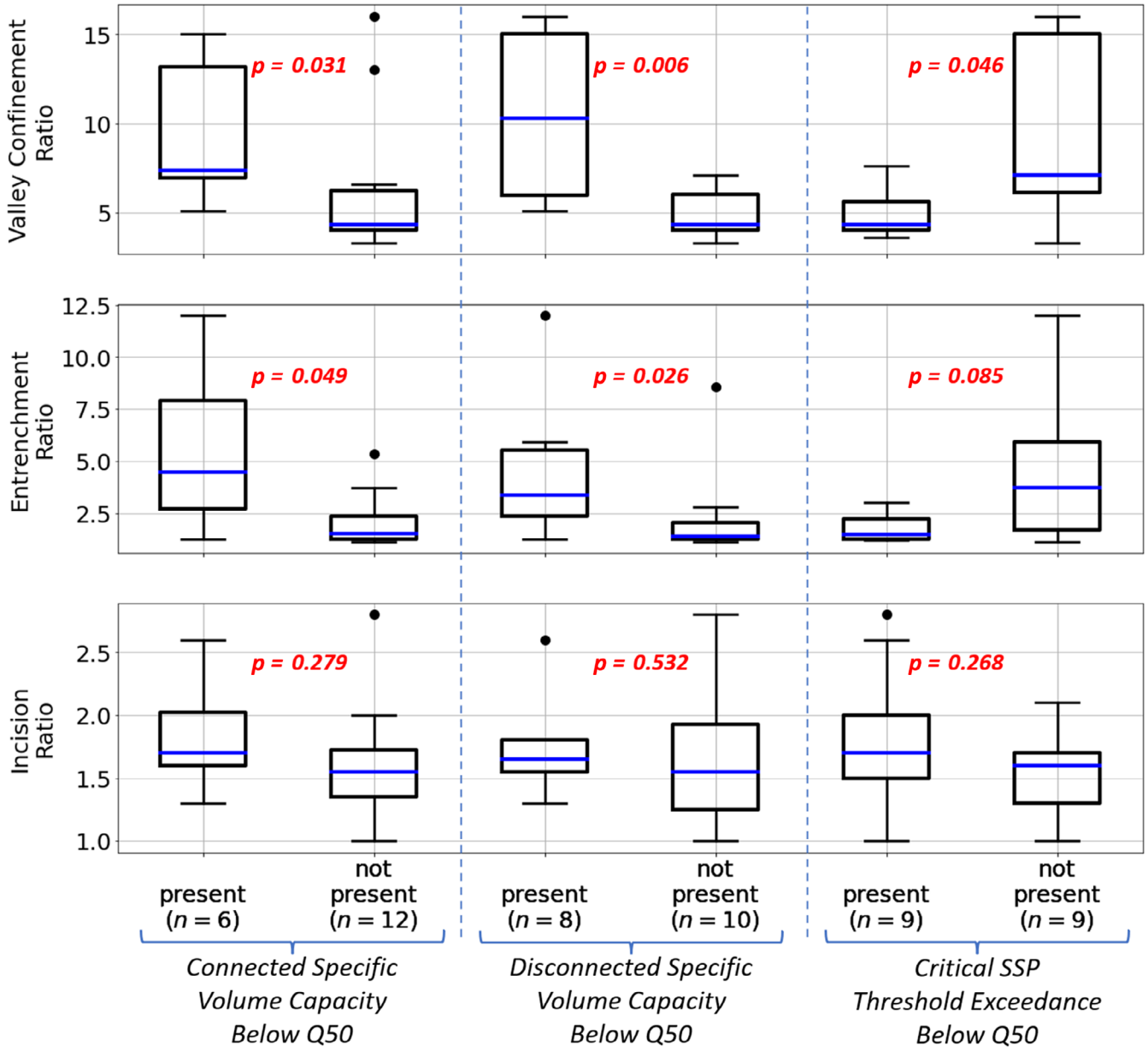

FIGURE 7 Comparison of valley confinement ratio, entrenchment ratio, and incision ratio to the disconnected specific volume capacity (DSVC), connected specific volume capacity (CSVC), and Critical specific stream power (Critical SSP) threshold exceedance measures. Reaches were separated into two groups based on presence or absence of three measures (CSVC, DSVC, and Critical SSP threshold exceedance) at discharge less than the Q50. For example, six reaches had CSVC below the Q50 threshold, and 12 reaches did not. We disregarded the presence of CVSC, DSVC, and Critical SSP threshold exceedances above the Q50. Boxes indicate sample medians and inner quartile range (IQR), and whiskers show the max (or min) values within 1.5*IQR above (or below) the box. The Kruskal–Wallis comparison of medians was used to calculate the *p* values. [Color figure can be viewed at wileyonlinelibrary.com]

between the channel and floodplain, all of which are needed to support healthy ecosystem function (Diehl et al., 2023; Opperman et al., 2010; Tockner & Stanford, 2002; Ward, 1989; Ward & Stanford, 1995). Conversely, reaches with substantial disconnected floodplain areas are likely to have degraded floodplain function.

Traditionally, pit-filling procedures consider pits as false artifacts that must be removed to route flow across the landscape (Lindsay, 2016; Soille, 2004; Wechsler, 2007). The more recent method of Aristizabal et al. (2022) includes the topography of pit-filled areas in order to improve the accuracy of flood inundation mapping, but we take this a step farther by utilizing pit information to highlight zones of DSVC. In the northeastern US and other regions where rivers and floodplains have been substantially modified (Blanton & Marcus, 2009; Scott et al., 2019), closed topographic depressions within the floodplain may be substantial in area and reflect true meso-topography of the landscape as modified by infrastructure encroachments. Unlike the method of Wilkinson et al. (2010), our method does not rely on known volumes of engineered features and can be applied

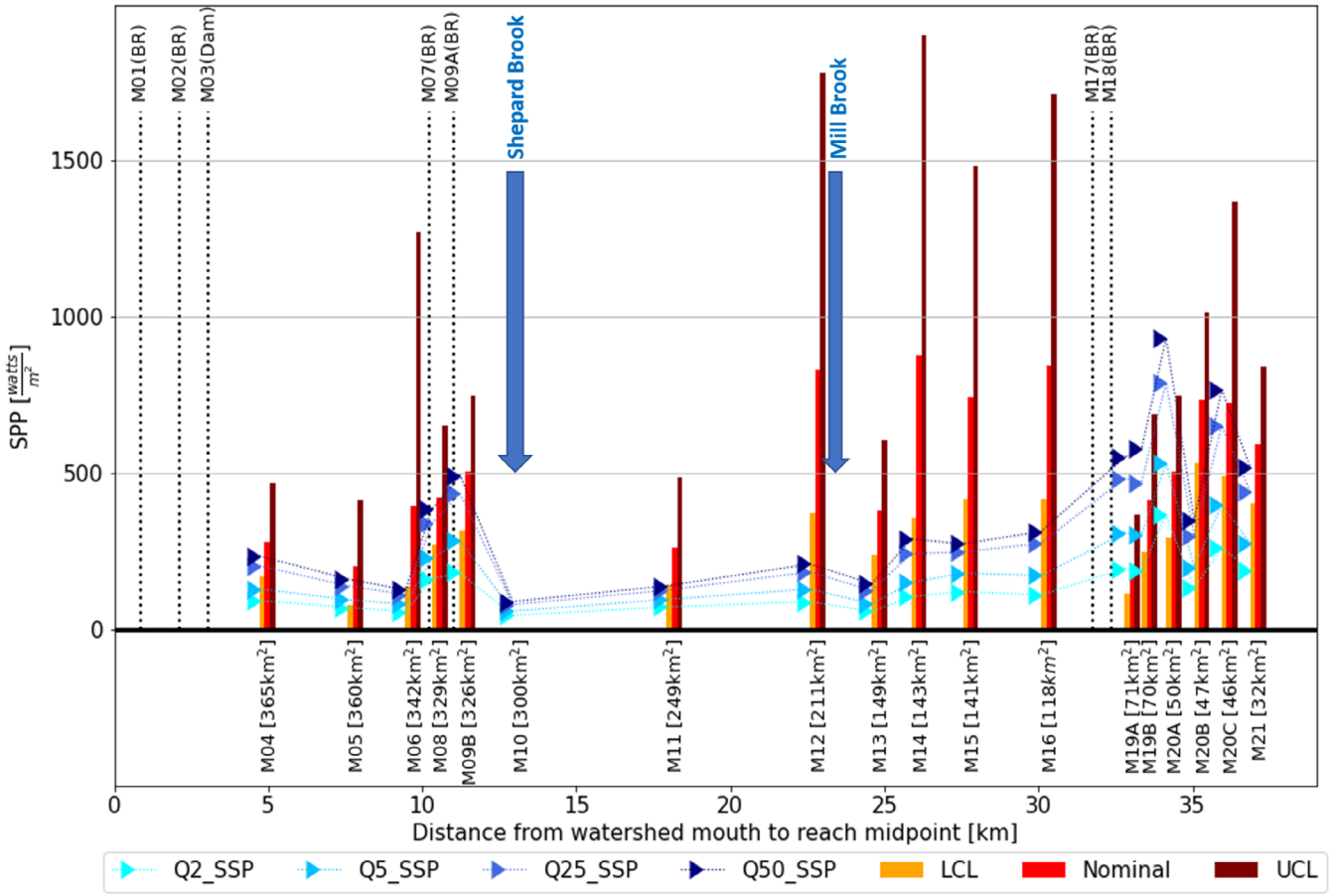

FIGURE 8 A longitudinal profile of design flood specific stream power (SSP) and SSP thresholds for alluvial reaches in the study area. Reach markers are placed at the midpoint of the reach as measured along the channel thalweg from the discharge point of the study area. Reach IDs and drainage areas are provided for each of the alluvial reaches. The design flood SSP values for each reach are indicated by triangular markers, and the SSP thresholds are represented by the bar graphs. The locations of the bedrock reaches and the dam-controlled reaches are indicated by vertical dotted lines. The vertical blue arrows indicate the location of major tributaries. LCL, lower confidence limit; UCL, upper confidence limit. [Color figure can be viewed at wileyonlinelibrary.com]

anywhere high-resolution DEMs are available. Restoration of these disconnected areas can significantly enhance floodplain functions, especially when evaluated and executed with respect to the larger watershed setting (Knox et al., 2022). In our study area, DSVC was typically dominated by larger, often anthropogenic pits, such as floodplains disconnected by the Route 100 road embankment. While values calculated for DSVC may also include the volume associated with smaller, often naturally occurring, pits (e.g., oxbow ponds) and noise in the DEMs (Lindsay, 2016), in our study, these were insignificant, typically accounting for <1 m^3/m of DSVC in any given reach.

4.2 | Broad-scale tools reveal watershed patterns

The ease with which these reach-based topographic signatures can be generated facilitates examination of downstream river dynamics within a watershed, as well as comparisons of watershed-scale patterns across regions. Bedrock reaches and dams (identified along the top of Figure 8) represent 'imposed controls' on channel and floodplain morphology and SSP (Khan et al., 2021; Stanford & Ward, 1993; Wohl, 2021). In a longitudinal context, these imposed controls represent fixed elevations or knick points that influence slope, sediment volumes, and grain size distributions. In a lateral context, these relatively short river reaches represent valley pinch points that influence hydraulics of floodwater flows (e.g., causing backwater effects) and cause discontinuities in sediment distribution. The intermediate alluvial or mixed reaches (identified along the bottom of Figure 8) are then influenced by 'flux controls' (Khan et al., 2021), including tributary junctions that deliver water and sediment on variable timings and development-related disturbances including removal of vegetation, encroachment of built infrastructure, and channel modifications (e.g., straightening, berming). These flux controls interact in nonlinear and complex ways to influence channel and floodplain morphology, which can in turn influence conveyance of floodwaters and sediment (Diehl et al., 2023; Macnab et al., 2006).

Accordingly, longitudinal patterns in the form-process measures emerged, suggesting general thresholds in river behavior and floodplain functions (Church, 2002). Exceedance of critical stream power was more common in headwater study area reaches (Figure 6, Table S.1), indicating the potential for upstream reaches to serve as a

production zone of sediment conveyed to depositional downstream reaches. Conversely, floodwater storage (both connected and disconnected) was available in reaches downstream of the production zone, indicating the initiation of floodplains (Jain et al., 2008).

Within our study region, we observed that the presence of connected floodplain storage areas correlated positively with VC. This was not unexpected, given the importance of valley confinement as a driving variable in the presence and extent of floodplains and as an important control on sediment deposition and flooding dynamics (Macnab et al., 2006; Van Appledorn et al., 2019). More specifically, the presence of floodwater storage areas (both connected and disconnected) is positively correlated with entrenchment ratio (ER; Figure 7). Some reaches are naturally confined by valley walls with negligible floodplain expression and therefore exhibit low ERs (<3). Other reaches have wide floodplains unconfined by valley walls but also exhibit entrenchment from: (1) built infrastructure (e.g., roads, rails, dense development) that encroaches the floodplain, (2) deep channel incision relative to its floodplain (so that floods are contained within the channel), or (3) a combination of both. In this sense, ER is a measure of both lateral and vertical (dis)connection of a channel to its floodplain, and our workflow provides a method to identify this entrenchment condition using remote sensing approaches, rather than labor-intensive field campaigns. Topographic signatures developed from sufficiently high-resolution DEMs and fine enough discretization of stage (0.1 m in this study), can reveal the reach entrenchment condition. Entrenched reaches (ER < 3) tend to show monotonically increasing SSP with stage, whereas nonentrenched reaches (ER > 3) tend to exhibit SSP-flow curves with gradual or abrupt energy dissipation features corresponding to connected or disconnected floodplain storage areas, respectively.

4.3 | Limitations and future work

The sample size used to develop our method and illustrate proof-of-concept is admittedly small and represents a subset of floodplain types. Our non-bedrock study reaches would be classified as 'equilibrium floodplains' by Nanson and Croke (1992), characterized by medium SSP (>10–300 watts/m^2) and non-cohesive boundaries in generally unconfined valley settings of moderate to low gradient. Expanded testing of these topographically based signatures across a wider range of geomorphic and hydrologic settings is the focus of future work to understand whether our process-form measures will correlate to geomorphic metrics in other lower energy settings.

There is potential for such process-form metrics to inform and improve reach- to watershed-scale routing of floodwaters within broad-scale flood prediction models (e.g., the National Water Model). Multi-date lidar or other topographic products could also be examined, at relatively low computational burden, to identify the influence of changing conditions over time. Scaling modeling and the accompanying datasets to the basin scale also aids in examining and parsing out complex interactions between reaches and emergent system behavior often obscured in site-scale analyses.

4.4 | River management implications

When combined, our process-form measures of floodplain connectivity and functioning provide insight into the feasibility of restoration or conservation projects for a given reach and can help planners prioritize projects at basin scales:

1. These measures, when evaluated at the watershed scale, can help identify river behavior zones. In the study area, floodplain restoration for floodwater, sediment, or nutrient storage would likely be most effective downstream of reach M17 (greater than approximately 90 km^2 of drainage area).
2. Reaches (i.e., M05, M19A, M19B, and M20; see Supplemental S.9) with SSP-flow curves that exceed critical SSP Thresholds at small design floods such as the Q5 (e.g., Figure 6, Note 1), may be good choices for restoration projects either at the reach itself or in upstream reaches to attenuate peak flows and dissipate flood energy and erosion/incision hazard (Gourevitch et al., 2020; Morris et al., 2005; Rijke et al., 2012).
3. Reaches (i.e., M06, M08, M11, M13, and M15) that have large DSVC accessed at small design floods or have CSVC accessed only at moderate design floods (Figure 6, Note 2) may be good choices for channel reconnection (e.g., berm lowering or removal; installation of cross-culverts beneath roads) (Morris et al., 2005; Worley et al., 2022).
4. Reaches with large CSVC that can be accessed at small design floods (i.e., M05, M08, M10, M11, M12, and M16) may be most suitable for conservation easements. These reaches (e.g., Figure 6, Note 3) are likely well-functioning and experience frequent water and sediment exchange. If the reach floodplains are currently in use by humans (e.g., agriculture, parks), these may also be good choices for restoration projects (e.g., planting trees, constructed wetlands) or removal of encroaching buildings or infrastructure (Gourevitch et al., 2020; Morris et al., 2005).

In practice, each of the above proposed actions would require a more detailed engineering analysis (and site-specific modeling) to assess whether the value provided by the restoration/conservation project outweighs the costs to society and environment and whether it addresses stakeholder goals (Rijke et al., 2012; Worley et al., 2023).

5 | CONCLUSIONS

In this study, we mined information on reach-scale river and floodplain character and behavior from readily available topographic datasets. We demonstrated that these measures can be used to quantify lateral/vertical (dis)connectivity and erosion hazards, information essential for targeting natural infrastructure (floodplain restoration and conservation) projects that are frequently lacking in watershed-scale planning efforts. Because our approach leverages a low-complexity hydraulic model based on publicly available datasets with

modest computational and setup costs, it can be more readily adopted at the regional level.

From the development of SSP-flow curves and application of erosion thresholds to a small watershed, we can conclude the following:

- Process-form measures describing channel-floodplain connectivity and fluvial erosion hazards can be calculated over a wide geographic area at relatively low computational and human labor costs compared to more hydraulically complex hydrodynamic models.
- Information embedded in DEMs and relative elevation products, such as HAND, may be used to describe the condition and function of rivers and floodplains.
- The suite of process-form measures presented captures both the natural variability imposed by the geomorphic setting, influencing the distribution of floodplain storage areas, energy dissipation zones, and fluvial erosion hazards, and the impact of built infrastructure and land use, highlighted by disconnected storage areas, abrupt spillovers, and high fluvial erosion hazards during regularly occurring floods.
- Our framework provides a useful measure to help planners choose areas for more detailed assessments of project feasibility. Synthesizing these measures into a reach classification framework may improve user friendliness for planners.

ACKNOWLEDGMENTS

JEM was funded by a Barrett Fellowship from the UVM GUND Institute of Environment, and DMR was supported in part by funding from NSF Vermont EPSCoR Grant Nos. EPS-1101317. This research was funded in part by grants from the Vermont Department of Environmental Conservation (LCW, KLU, RMD, and KSL), Lake Champlain Sea Grant (LCW, KLU, DMR, and RMD), and the University of Alabama (RMD, KLU, KSL, and DMR). Research was supported in part using federal funds under Award NA18OAR4170099 to Lake Champlain Sea Grant from the National Oceanic and Atmospheric Administration National Sea Grant College Program, and through the NOAA cooperative agreement with Alabama (Award NA22NWS4320003). The statements, findings, conclusions, and recommendations are those of the author(s) and do not necessarily reflect the views of NSF, Sea Grant, NOAA. The authors are grateful to Mike Kline, Evelyn Boardman, Roy Schiff, and Evan Fitzgerald of the Vermont Functioning Floodplain Initiative for feedback regarding the SSP-flow curves and critical SSP thresholds. Stephi Drago aided with DEM hydroenforcing and preparation of probHAND inputs, including StreamStats flow rates and SGA stream polylines.

CONFLICT OF INTEREST STATEMENT

The authors, to the best of their knowledge, are not aware of any conflicts of interest.

DATA AVAILABILITY STATEMENT

All data in this work are publicly available (see Supplemental S.2). The Python code for this work is available on Github: https://github.com/jeremymatt/terrain_derived_connectivity_measures.

ORCID

Jeremy E. Matt https://orcid.org/0000-0003-1857-0434
Kristen L. Underwood https://orcid.org/0000-0003-3008-3057
Rebecca M. Diehl https://orcid.org/0000-0001-9414-4045
Lindsay C. Worley https://orcid.org/0000-0003-2773-578X
Donna M. Rizzo https://orcid.org/0000-0003-4123-5028

REFERENCES

Acreman, M. C., Riddington, R., & Booker, D. J. (2003). Hydrological impacts of floodplain restoration: A case study of the River Cherwell, UK. *Hydrology and Earth System Sciences*, *7*(1), 75–85. https://doi.org/10.5194/hess-7-75-2003

Ahilan, S., Guan, M., Sleigh, A., Wright, N., & Chang, H. (2018). The influence of floodplain restoration on flow and sediment dynamics in an urban river. *Journal of Flood Risk Management*, *11*(S2), S986–S1001. https://doi.org/10.1111/jfr3.12251

Ahmad, I. (2018). Digital elevation model (DEM) coupled with geographic information system (GIS): An approach towards erosion modeling of Gumara watershed, Ethiopia. *Environmental Monitoring and Assessment*, *190*(10), 568. https://doi.org/10.1007/s10661-018-6888-8

Akanbi, A. A., Lian, Y., & Soong, T. W. (1999). An analysis on managed flood storage options for selected levees along the lower Illinois River for enhancing flood protection (no. 4). In *Flood storage reservoirs and flooding on the lower Illinois River* (p. 89). Office of Water Resources Illinois Department of Natural Resources. https://core.ac.uk/download/pdf/158316874.pdf

Alexander, G. G., & Allan, J. D. (2007). Ecological success in stream restoration: Case studies from the midwestern United States. *Environmental Management*, *40*(2), 245–255. https://doi.org/10.1007/s00267-006-0064-6

Andrews, E. D. (1983). Entrainment of gravel from naturally sorted riverbed material. *Geological Society of America Bulletin*, *94*(10), 1225. https://doi.org/10.1130/0016-7606(1983)94<1225:EOGFNS>2.0.CO;2

Aristizabal, F., Petrochenkov, G., Salas, F., Zamanisabzi, H., Luck, M., Avant, B., Bates, B., Grout, T., Spies, R., Chadwick, N., Wills, Z., & Judge, J. (2022). Reducing a stream network's Horton-Strahler stream order improves the skill of flood inundation maps from height above nearest drainage method. Hydrology. https://doi.org/10.1002/essoar.10510488.1

Bagnold, R. A. (1966). *An approach to the sediment transport problem from general physics*. Geological Survey Professional Paper 422-I (p. 49). United States Government Printing Office.

Beck, W. J., Moore, P. L., Schilling, K. E., Wolter, C. F., Isenhart, T. M., Cole, K. J., & Tomer, M. D. (2019). Changes in lateral floodplain connectivity accompanying stream channel evolution: Implications for sediment and nutrient budgets. *Science of the Total Environment*, *660*, 1015–1028. https://doi.org/10.1016/j.scitotenv.2019.01.038

Bizzi, S., & Lerner, D. N. (2015). The use of stream power as an indicator of channel sensitivity to erosion and deposition processes. *River Research and Applications*, *31*(1), 16–27. https://doi.org/10.1002/rra.2717

Blanton, P., & Marcus, W. A. (2009). Railroads, roads and lateral disconnection in the river landscapes of the continental United States. *Geomorphology*, *112*(3–4), 212–227. https://doi.org/10.1016/j.geomorph.2009.06.008

Booth, D. B. (1990). Stream-channel incision following drainage-basin urbanization. *JAWRA Journal of the American Water Resources Association*, *26*(3), 407–417. https://doi.org/10.1111/j.1752-1688.1990.tb01380.x

Castellarin, A., Di Baldassarre, G., & Brath, A. (2011). Floodplain management strategies for flood attenuation in the river Po. *River Research and Applications*, *27*(8), 1037–1047. https://doi.org/10.1002/rra.1405

Church, M. (2002). Geomorphic thresholds in riverine landscapes: Geomorphic thresholds. *Freshwater Biology*, *47*(4), 541–557. https://doi.org/10.1046/j.1365-2427.2002.00919.x

Danielson, T. (2013). *Utilizing a high resolution digital elevation model (DEM) to develop a stream power index (SPI) for the Gilmore Creek watershed in Winona County, Minnesota Papers in resource analysis* (Vol. 15). Saint Mary's University of Minnesota University Central Services Press.

Diehl, R. M., Gourevitch, J. D., Drago, S., & Wemple, B. C. (2021). Improving flood hazard datasets using a low-complexity, probabilistic floodplain mapping approach. *PLoS One*, *16*(3), e0248683. https://doi.org/10.1371/journal.pone.0248683

Diehl, R. M., Underwood, K. L., Triantafillou, S. P., Ross, D. S., Drago, S., & Wemple, B. C. (2023). Multi-scale drivers of spatial patterns in floodplain sediment and phosphorus deposition. *Earth Surface Processes and Landforms*, *48*(4), 801–816. https://doi.org/10.1002/esp.5519

Eaton, B. C., Moore, R. D., & MacKenzie, L. G. (2019). Percentile-based grain size distribution analysis tools (GSDtools) – Estimating confidence limits and hypothesis tests for comparing two samples. *Earth Surface Dynamics*, *7*(3), 789–806. https://doi.org/10.5194/esurf-7-789-2019

Ferguson, R. I. (2005). Estimating critical stream power for bedload transport calculations in gravel-bed rivers. *Geomorphology*, *70*(1–2), 33–41. https://doi.org/10.1016/j.geomorph.2005.03.009

Fitzgerald, E. P., & Godfrey, L. C. (2008). *Upper Mad River corridor plan January 31, 2008* (p. 117). Fitzgerald Environmental Associates, LLC.

Gartner, J. D., Dade, W. B., Renshaw, C. E., Magilligan, F. J., & Buraas, E. M. (2015). Gradients in stream power influence lateral and downstream sediment flux in floods. *Geology*, *43*(11), 983–986. https://doi.org/10.1130/G36969.1

Gleason, R. A., Tangen, B. A., Laubhan, M. K., Kermes, K. E., & Euliss, N. H., Jr. (2007). *Estimating water storage capacity of existing and potentially restorable wetland depressions in a subbasin of the Red River of the north: U.S. Geological Survey open-file report 2007–1159* (Open-File Report No. 2007–1159; Open-File Report, p. 36). U.S. Geological Survey. https://digitalcommons.unl.edu/cgi/viewcontent.cgi?article=1106&context=usgsnpwrc

Gourevitch, J. D., Diehl, R. M., Wemple, B. C., & Ricketts, T. H. (2022). Inequities in the distribution of flood risk under floodplain restoration and climate change scenarios. *People and Nature*, *4*(2), 415–427. https://doi.org/10.1002/pan3.10290

Gourevitch, J. D., Singh, N. K., Minot, J., Raub, K. B., Rizzo, D. M., Wemple, B. C., & Ricketts, T. H. (2020). Spatial targeting of floodplain restoration to equitably mitigate flood risk. *Global Environmental Change*, *61*, 102050. https://doi.org/10.1016/j.gloenvcha.2020.102050

Grauso, S., Pasanisi, F., & Tebano, C. (2018). Assessment of a simplified connectivity index and specific sediment potential in river basins by means of geomorphometric tools. *Geosciences*, *8*(2), 48. https://doi.org/10.3390/geosciences8020048

Hermoso, V., Pantus, F., Olley, J., Linke, S., Mugodo, J., & Lea, P. (2012). Systematic planning for river rehabilitation: Integrating multiple ecological and economic objectives in complex decisions. *Freshwater Biology*, *57*(1), 1–9. https://doi.org/10.1111/j.1365-2427.2011.02693.x

Holman-Dodds, J. K., Bradley, A. A., & Potter, K. W. (2003). Evaluation of hydrologic benefits of infiltration based urban storm water management. *JAWRA Journal of the American Water Resources Association*, *39*(1), 205–215. https://doi.org/10.1111/j.1752-1688.2003.tb01572.x

Jain, V., Fryirs, K., & Brierley, G. (2008). Where do floodplains begin? The role of total stream power and longitudinal profile form on floodplain initiation processes. *Geological Society of America Bulletin*, *120*(1–2), 127–141. https://doi.org/10.1130/B26092.1

Jain, V., Preston, N., Fryirs, K., & Brierley, G. (2006). Comparative assessment of three approaches for deriving stream power plots along long profiles in the upper Hunter River catchment, New South Wales, Australia. *Geomorphology*, *74*(1–4), 297–317. https://doi.org/10.1016/j.geomorph.2005.08.012

Jones, J. A., Swanson, F. J., Wemple, B. C., & Snyder, K. U. (2000). Effects of roads on hydrology, geomorphology, and disturbance patches in stream networks. *Conservation Biology*, *14*(1), 76–85. https://doi.org/10.1046/j.1523-1739.2000.99083.x

Juan, A., Gori, A., & Sebastian, A. (2020). Comparing floodplain evolution in channelized and unchannelized urban watersheds in Houston, Texas. *Journal of Flood Risk Management*, *13*(2), e12604. https://doi.org/10.1111/jfr3.12604

Khan, S., Fryirs, K. A., & Ralph, T. J. (2021). Geomorphic controls on the diversity and patterns of fluvial forms along longitudinal profiles. *Catena*, *203*, 105329. https://doi.org/10.1016/j.catena.2021.105329

Kline, M., & Cahoon, B. (2010). Protecting river corridors in Vermont. *JAWRA Journal of the American Water Resources Association*, *46*(2), 227–236. https://doi.org/10.1111/j.1752-1688.2010.00417.x

Kline, M., Alexander, C., Pytlik, S., & Pomeroy, S. (2009). *Vermont stream geomorphic assessment phase II handbook: Rapid stream assessment*. VTANR. https://dec.vermont.gov/sites/dec/files/wsm/rivers/docs/rv_SGA_Phase2_Protocol.pdf

Knighton, A. D. (1999). Downstream variation in stream power. *Geomorphology*, *29*(3), 293–306. https://doi.org/10.1016/S0169-555X(99)00015-X

Knox, R. L., Wohl, E. E., & Morrison, R. R. (2022). Levees don't protect, they disconnect: A critical review of how artificial levees impact floodplain functions. *Science of the Total Environment*, *837*, 155773. https://doi.org/10.1016/j.scitotenv.2022.155773

Kvočka, D., Ahmadian, R., & Falconer, R. A. (2018). Predicting flood hazard indices in torrential or flashy river basins and catchments. *Water Resources Management*, *32*(7), 2335–2352. https://doi.org/10.1007/s11269-018-1932-6

Lane, S. N. (2017). Natural flood management. *WIREs Water*, *4*(3), e1211. https://doi.org/10.1002/wat2.1211

Lane, S. N., Reaney, S. M., & Heathwaite, A. L. (2009). Representation of landscape hydrological connectivity using a topographically driven surface flow index. *Water Resources Research*, *45*(8), 1–10. https://doi.org/10.1029/2008WR007336

Lindsay, J. B. (2016). Efficient hybrid breaching-filling sink removal methods for flow path enforcement in digital elevation models. *Hydrological Processes*, *30*(6), 846–857. https://doi.org/10.1002/hyp.10648

Lisenby, P. E., Croke, J., & Fryirs, K. A. (2018). Geomorphic effectiveness: A linear concept in a non-linear world: Geomorphic effectiveness. *Earth Surface Processes and Landforms*, *43*(1), 4–20. https://doi.org/10.1002/esp.4096

Macnab, K., Jacobson, C., & Brierley, G. (2006). Spatial variability of controls on downstream patterns of sediment storage: A case study in the Lane Cove Catchment, New South Wales, Australia. *Geographical Research*, *44*(3), 255–271. https://doi.org/10.1111/j.1745-5871.2006.00388.x

Magilligan, F. J. (1992). Thresholds and the spatial variability of flood power during extreme floods. *Geomorphology*, *5*(3–5), 373–390. https://doi.org/10.1016/0169-555X(92)90014-F

Magilligan, F. J., Buraas, E. M., & Renshaw, C. E. (2015). The efficacy of stream power and flow duration on geomorphic responses to catastrophic flooding. *Geomorphology*, *228*, 175–188. https://doi.org/10.1016/j.geomorph.2014.08.016

Marcinkowski, P., Kiczko, A., & Kardel, I. (2022). Large-scale assessment of spatial variability in stream power distribution: An indicator of channel erosion and deposition potential. *Journal of Hydrology*, *605*, 127319. https://doi.org/10.1016/j.jhydrol.2021.127319

Morris, J., Hess, T. M., Gowing, D. J. G., Leeds-Harrison, P. B., Bannister, N., Vivash, R. M. N., & Wade, M. (2005). A framework for integrating flood defence and biodiversity in washlands in England. *International Journal of River Basin Management*, *3*(2), 105–115. https://doi.org/10.1080/15715124.2005.9635250

Morris, J., Hess, T. M., Gowing, D. J., Leeds-Harrison, P. B., Bannister, N., Wade, M., & Vivash, R. M. (2004). *Integrated washland management for flood defence and biodiversity* (Report No. 598). English Nature Research Reports. https://dspace.lib.cranfield.ac.uk/handle/1826/1207

Nanson, G. C., & Croke, J. C. (1992). A genetic classification of floodplains. *Geomorphology*, *4*(6), 459–486. https://doi.org/10.1016/0169-555X(92)90039-Q

Nilsson, C., Reidy, C. A., Dynesius, M., & Revenga, C. (2005). Fragmentation and flow regulation of the world's large river systems. *Science*, *308*(5720), 405–408. https://doi.org/10.1126/science.1107887

Nobre, A. D., Cuartas, L. A., Hodnett, M., Rennó, C. D., Rodrigues, G., Silveira, A., Waterloo, M., & Saleska, S. (2011). Height above the nearest drainage – A hydrologically relevant new terrain model. *Journal of Hydrology*, *404*(1–2), 13–29. https://doi.org/10.1016/j.jhydrol.2011.03.051

Noe, G. B., & Hupp, C. R. (2009). Retention of riverine sediment and nutrient loads by coastal plain floodplains. *Ecosystems*, *12*(5), 728–746. https://doi.org/10.1007/s10021-009-9253-5

O'Sullivan, J. J., Ahilan, S., & Bruen, M. (2012). A modified Muskingum routing approach for floodplain flows: Theory and practice. *Journal of Hydrology*, *470–471*, 239–254. https://doi.org/10.1016/j.jhydrol.2012.09.007

Olson, S. A. (2014). *Estimation of flood discharges at selected annual exceedance probabilities for unregulated, rural streams in Vermont* (Scientific Investigations Report, p. 37) [Scientific Investigations Report]. United States Geological Survey. https://pubs.usgs.gov/sir/2014/5078/pdf/sir2014-5078.pdf

Opperman, J. J., Luster, R., McKenney, B. A., Roberts, M., & Meadows, A. W. (2010). Ecologically functional floodplains: Connectivity, flow regime, and scale. *JAWRA Journal of the American Water Resources Association*, *46*(2), 211–226. https://doi.org/10.1111/j.1752-1688.2010.00426.x

Reinfelds, I., Cohen, T., Batten, P., & Brierley, G. (2004). Assessment of downstream trends in channel gradient, total and specific stream power: A GIS approach. *Geomorphology*, *60*(3–4), 403–416. https://doi.org/10.1016/j.geomorph.2003.10.003

Rijke, J., van Herk, S., Zevenbergen, C., & Ashley, R. (2012). Room for the river: Delivering integrated river basin management in The Netherlands. *International Journal of River Basin Management*, *10*(4), 369–382. https://doi.org/10.1080/15715124.2012.739173

Roni, P., Hanson, K., & Beechie, T. (2008). Global review of the physical and biological effectiveness of stream habitat rehabilitation techniques. *North American Journal of Fisheries Management*, *28*, 856–890. https://doi.org/10.1577/M06-169.1

Ross, D. S., Wemple, B. C., Willson, L. J., Balling, C. M., Underwood, K. L., & Hamshaw, S. D. (2019). Impact of an extreme storm event on river corridor bank erosion and phosphorus mobilization in a mountainous watershed in the northeastern United States. *Journal of Geophysical Research – Biogeosciences*, *124*(1), 18–32. https://doi.org/10.1029/2018JG004497

Schoof, R. (1980). Environmental impact of channel modification. *JAWRA Journal of the American Water Resources Association*, *16*(4), 697–701. https://doi.org/10.1111/j.1752-1688.1980.tb02451.x

SciPy (1.3). (2019). Open-source software for mathematics, science, and engineering. https://scipy.org/

Scott, D. T., Gomez-Velez, J. D., Jones, C. N., & Harvey, J. W. (2019). Floodplain inundation spectrum across the United States. *Nature Communications*, *10*(1), 5194. https://doi.org/10.1038/s41467-019-13184-4

Seigel, R. (2021). *Flood analysis of bridge-stream interactions using two-dimensional models* [masters]. University of Vermont.

Shankman, D., & Pugh, T. (1992). Discharge response to channelization of a coastal plain stream. *Wetlands*, *12*, 157–162. https://doi.org/10.1007/BF03160604

Simon, A., & Rinaldi, M. (2006). Disturbance, stream incision, and channel evolution: The roles of excess transport capacity and boundary materials in controlling channel response. *Geomorphology*, *79*(3), 361–383. https://doi.org/10.1016/j.geomorph.2006.06.037

Soille, P. (2004). Optimal removal of spurious pits in grid digital elevation models. *Water Resources Research*, *40*(12), 1–9. https://doi.org/10.1029/2004WR003060

Stanford, J. A., & Ward, J. V. (1993). An ecosystem perspective of alluvial rivers: Connectivity and the hyporheic corridor. *Journal of the North American Benthological Society*, *12*(1), 48–60. https://doi.org/10.2307/1467685

Tarboton, D. (2016). *TauDEM* (5.3.7). https://hydrology.usu.edu/taudem/taudem5/

Tockner, K., & Stanford, J. A. (2002). Riverine flood plains: Present state and future trends. *Environmental Conservation*, *29*(3), 308–330. https://doi.org/10.1017/S037689290200022X

Underwood, K. L., Rizzo, D. M., Dewoolkar, M. M., & Kline, M. (2021). Analysis of reach-scale sediment process domains in glacially-conditioned catchments using self-organizing maps. *Geomorphology*, *382*, 107684. https://doi.org/10.1016/j.geomorph.2021.107684

Van Appledorn, M., Baker, M. E., & Miller, A. J. (2019). River-valley morphology, basin size, and flow-event magnitude interact to produce wide variation in flooding dynamics. *Ecosphere*, *10*(1), 1–15. https://doi.org/10.1002/ecs2.2546

VTANR. (2022). *Stream geomorphic assessment data management system* [Data set]. https://anrweb.vt.gov/DEC/SGA/Default.aspx

Ward, J. V. (1989). The four-dimensional nature of lotic ecosystems. *Journal of the North American Benthological Society*, *8*(1), 2–8. https://doi.org/10.2307/1467397

Ward, J. V., & Stanford, J. A. (1995). Ecological connectivity in alluvial river ecosystems and its disruption by flow regulation. *Regulated Rivers: Research & Management*, *11*(1), 105–119. https://doi.org/10.1002/rrr.3450110109

Wechsler, S. P. (2007). Uncertainties associated with digital elevation models for hydrologic applications: A review. *Hydrology and Earth System Sciences*, *11*(4), 1481–1500. https://doi.org/10.5194/hess-11-1481-2007

Wilkinson, M. E., Quinn, P. F., & Welton, P. (2010). Runoff management during the September 2008 floods in the Belford catchment, Northumberland: Runoff management during a flood event in Northumberland. *Journal of Flood Risk Management*, *3*(4), 285–295. https://doi.org/10.1111/j.1753-318X.2010.01078.x

Wilson, A. L., Dehaan, R. L., Watts, R. J., Page, K. J., Bowmer, K. H., & Curtis, A. (2007). *Proceedings of the 5th Australian Stream Management Conference*. Australian rivers: making a difference. Charles Sturt University, Thurgoona, New South Wales.

Wohl, E. (2017). The significance of small streams. *Frontiers of Earth Science*, *11*(3), 447–456. https://doi.org/10.1007/s11707-017-0647-y

Wohl, E. (2021). An integrative conceptualization of floodplain storage. *Reviews of Geophysics*, *59*(2), e2020RG000724. https://doi.org/10.1029/2020RG000724

Wolff, C. G., & Burges, S. J. (1994). An analysis of the influence of river channel properties on flood frequency. *Journal of Hydrology*, *153*(1–4), 317–337. https://doi.org/10.1016/0022-1694(94)90197-X

Worley, L. C., Underwood, K. L., Diehl, R. M., Matt, J. E., Lawson, K. S., Seigel, R. M., & Rizzo, D. M. (2023). Balancing multiple stakeholder objectives for floodplain reconnection and wetland restoration. *Journal of Environmental Management*, *326*, 116648. https://doi.org/10.1016/j.jenvman.2022.116648

Worley, L. C., Underwood, K. L., Vartanian, N. L. V., Dewoolkar, M. M., Matt, J. E., & Rizzo, D. M. (2022). Semi-automated hydraulic model wrapper to support stakeholder evaluation: A floodplain reconnection study using 2D hydrologic engineering center's river analysis system. *River Research and Applications*, *38*(4), 799–809. https://doi.org/10.1002/rra.3946

Zheng, X., Tarboton, D. G., Maidment, D. R., Liu, Y. Y., & Passalacqua, P. (2018). River channel geometry and rating curve estimation using height above the nearest drainage. *JAWRA Journal of the American Water Resources Association*, *54*(4), 785–806. https://doi.org/10.1111/1752-1688.12661

SUPPORTING INFORMATION

Additional supporting information can be found online in the Supporting Information section at the end of this article.

How to cite this article: Matt, J. E., Underwood, K. L., Diehl, R. M., Lawson, K. S., Worley, L. C., & Rizzo, D. M. (2023). Terrain-derived measures for basin conservation and restoration planning. *River Research and Applications*, *39*(9), 1795–1811. https://doi.org/10.1002/rra.4181